

# Crystal structures and phase transformation of deuterated lithium imide, $\text{Li}_2\text{ND}$

Michael P. Balogh<sup>a,\*</sup>, Camille Y. Jones<sup>b</sup>, J.F. Herbst<sup>c</sup>,  
Louis G. Hector Jr.<sup>c</sup>, Matthew Kundrat<sup>d</sup>

<sup>a</sup> Chemical and Environmental Sciences Laboratory, General Motors Research and Development Center,  
30500 Mound Road, Warren, MI 48090-9055, United States

<sup>b</sup> NIST Center for Neutron Research, 100 Bureau Drive, Stop 8562, National Institute of Standards and Technology,  
Gaithersburg, MD 20899-8562, United States

<sup>c</sup> Materials and Processes Laboratory, General Motors Research and Development Center,  
30500 Mound Road, Warren, MI 48090-9055, United States

<sup>d</sup> Aerotek Corp., 26211 Central Park Blvd., Southfield, MI 48076, United States

Received 17 October 2005; received in revised form 3 November 2005; accepted 4 November 2005

Available online 28 December 2005

## Abstract

We have investigated the crystal structure of deuterated lithium imide,  $\text{Li}_2\text{ND}$ , by means of neutron and X-ray diffraction. An order–disorder transition occurs near 360 K. Below that temperature  $\text{Li}_2\text{ND}$  can be described to the same level of accuracy as a disordered cubic ( $Fd\bar{3}m$ ) structure with partially occupied Li 32e sites or as a fully occupied orthorhombic ( $Ima2$  or  $Imm2$ ) structure. The high temperature phase is best characterized as disordered cubic ( $Fm\bar{3}m$ ) with D atoms randomized over the 192i sites. Density functional theory calculations complement and support the diffraction analyses. We compare our findings in detail with previous studies.

© 2005 Elsevier B.V. All rights reserved.

**Keywords:** Hydrogen absorbing materials; Crystal structure; Neutron diffraction; X-ray diffraction; Order–disorder effects

## 1. Introduction

The pursuit of a practical method for the storage of hydrogen for fuel has brought to prominence many long forgotten compounds and chemistries. This is particularly true in the case of lithium imide,  $\text{Li}_2\text{NH}$ . Although the synthesis of  $\text{Li}_2\text{NH}$  was described as early as 1911 [1,2], only recently has interest in  $\text{Li}_2\text{NH}$  been renewed when it was identified as an intermediate formed during the hydrogenation of lithium nitride ( $\text{Li}_3\text{N}$ ) [3]. In theory,  $\text{Li}_2\text{NH}$  can store up to 6.5 wt.% hydrogen reversibly at temperatures lower than 300 °C. Motivated by this insight, the discovery of a whole new class of hydrogen storage materials has resulted and has since stimulated new research into  $\text{Li}_2\text{NH}$  and similar compounds. Much of this research has focused on the dehydrogenation mechanism in the  $\text{Li}_2\text{NH}$  system [4,5]. However, little has been offered in terms of a mechanism of

hydrogenation, in large part owing to the lack of an accurate crystal structure.

The first proposed crystal structure identified  $\text{Li}_2\text{NH}$  as iso-morphous with  $\text{Li}_2\text{O}$ , an anti-fluorite structure with  $[\text{NH}]^{2-}$  groups in rotation and thus possessing spherical symmetry, but did not include the atomic positions of the hydrogens [6]. More recently, Ohoyama et al. [7] performed neutron powder diffraction experiments on  $\text{Li}_2\text{NH}$  and proposed a revised crystal structure model with a face-centered cubic (fcc) symmetry in space group  $F\bar{4}3m$ . They chose a structure model with random occupancy of H atoms on four of the tetrahedrally arranged 16e sites surrounding a N site at a distance of 0.82(6) Å from the N atom. Most recently, Noritake et al. [8] performed X-ray powder diffraction experiments and charge density analysis of  $\text{Li}_2\text{NH}$ . They also proposed an fcc structure but in space group  $Fm\bar{3}m$ . In their model the H atoms are randomized over 4 of the 48 h sites surrounding a N site at a distance of 0.80(16) Å from the N atom. The works of Ohoyama et al. and Noritake et al. propose different crystal structures; however, in both cases the proposed structures were statistically indistinguishable from other crystal structure

\* Corresponding author. Tel.: +1 586 986 0862; fax: +1 586 986 0817.  
E-mail address: michael.p.balogh@gm.com (M.P. Balogh).

models they considered in their respective investigations. Therefore, both papers resorted to secondary considerations such as interatomic distances and symmetry in the selection of their proposed model. Although differences do exist between the three models mentioned above, all of the models draw the same conclusion, i.e., that of a structure containing fully occupied N and Li sites with disorder due to random occupancy of H sites. We note, however, that disordered structures appear qualitatively inconsistent with the report [9] of an order–disorder transition in  $\text{Li}_2\text{NH}$  observed by differential scanning calorimetry (DSC) at 356 K and with the known ordered structure of the related compound  $\text{LiNH}_2$ , lithium amide.

In order to resolve the ambiguity in the crystal structure of  $\text{Li}_2\text{NH}$  and to determine more precisely the positions of the H atoms, we have synthesized the fully deuterated form of this compound and measured its neutron powder diffraction patterns at several temperatures. The measurement of deuterated material reduces the incoherent scattering from H, increases the overall intensity in the Bragg reflections, and produces reflections at high scattering angles which are not diminished by a  $(\sin \theta/\lambda)$  dependence of the scattering length, and is thus the preferred method for determining the crystal structure of hydrogenated materials. For comparison, the bound coherent scattering lengths for Li, N, H, and  $^2\text{H}$  are  $-1.90(2)$ ,  $9.36(2)$ ,  $-3.7390(11)$ , and  $6.671(4)$ , respectively, in units of barns ( $1 \text{ barn} = 100 \text{ fm}^2$ ) [10]. Moreover, to assist discrimination among possible structures, X-ray powder diffraction experiments and density functional theory (DFT) calculations of electronic total energies were performed as well.

## 2. Experimental

### 2.1. Synthesis

A sample of  $\text{Li}_2\text{ND}$  ( $\text{Li}_2\text{N}^2\text{H}$ ) was prepared using a variation of the method described by Juza and Opp [6], with some minor modifications made so the synthesis could be performed in a closed system:



The reactions were carried out in a stainless steel pressure vessel (Parr) [11]; all other procedures were performed in an argon-filled glove box. Clean lithium metal ribbon (99.9%) was placed in the upper of two nested nickel crucibles. The upper crucible contained several small holes, thus allowing the molten  $\text{LiND}_2$  formed in reaction (2) to flow into the bottom crucible. After being sealed and removed from the glove box, the reactor was evacuated and nitrogen (99.998%) was supplied at 900 kPa. Because of the exothermic nature of reaction (1), the temperature rose immediately. Once the vessel cooled and the nitrogen had been evacuated, deuterated ammonia (99 atom% D) was supplied at 800 kPa while the vessel was slowly heated to 673 K. Once the ammonia ceased to be consumed, the reactor was cooled to 633 K and held under vacuum for 3 h. The temperature was then slowly increased to 723 K. After 2 h, the reactor was allowed to cool in the furnace. Subsequent diffraction experiments detected no lithium oxide ( $\text{Li}_2\text{O}$ ), lithium amide ( $\text{LiND}_2$ ), or lithium nitride ( $\text{Li}_3\text{N}$ ). Chemical analysis of the product found 47.9 wt.% Li (theoretical 46.4 wt.%), 45.1 wt.% N (theoretical 46.9 wt.%), 6.72 wt.% D (theoretical 6.69 wt.%), and 0.4 wt.% C. DSC experiments (cf. Fig. 1) confirmed that the product also undergoes a reversible phase transformation at 358 K, with a hysteresis of 5 K.

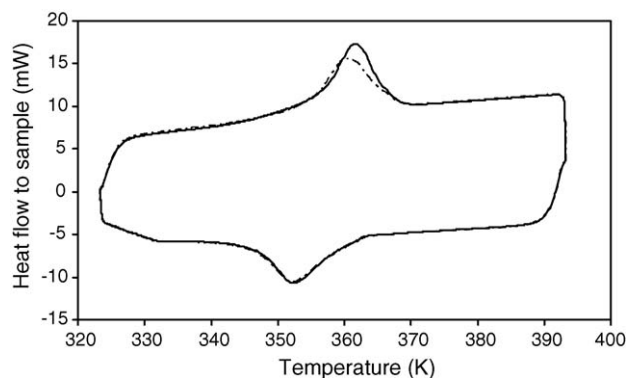


Fig. 1. Differential scanning calorimetry data for  $\text{Li}_2\text{ND}$ .

### 2.2. Neutron powder diffraction

Data were collected on the BT-1 32-detector neutron powder diffractometer at the National Institute of Standards and Technology's NIST Center for Neutron Research (NCNR) [12]. A  $\text{Cu}(311)$  monochromator with a wavelength of  $1.5402 \text{ \AA}$  was employed, the take-off angle was  $90^\circ$ , and the in-pile collimation was  $15 \text{ min of arc}$ . The instrument configuration employed for this study allowed data to be collected over the range  $0.25 \text{ \AA}^{-1} < Q < 6 \text{ \AA}^{-1}$ . The beam was masked to  $1.59 \text{ cm} \times 5.08 \text{ cm}$  at the sample. Measurements were made on  $\sim 10 \text{ g}$  of material in a vanadium can of length  $5.08 \text{ cm}$  and outer diameter  $1.56 \text{ cm}$ . Data were collected over the range of  $3^\circ < 2\theta < 165^\circ$  with a step size of  $0.05^\circ 2\theta$  at 100, 200, 300, and 400 K with equilibration times of 15 min. Once the occurrence of a phase transformation became apparent, 1-h measurements were made in the direction of decreasing temperature to further establish the transformation temperature.

### 2.3. X-ray powder diffraction

X-ray diffraction data were collected at room temperature using  $\text{Cu K}\alpha$  radiation with a Siemens D5000 powder diffractometer configured in parallel-beam geometry using a Göbel mirror primary beam monochromator and  $0.15^\circ$  Soller slits. The sample was packed into a sample holder and sealed with an  $8 \mu\text{m}$  thick Kapton film. The film did not fully seal the sample; therefore, to detect contamination of the specimen by air, eight diffraction patterns were collected serially. Each diffraction pattern was measured at a fixed incidence angle of  $5^\circ$  with a step size of  $0.02^\circ$  and a counting time of 1 s/step. A small increase in the amount of  $\text{LiOH}$  was observed with each subsequent diffraction pattern. A crystal structure refinement was performed on the compilation of all eight diffraction patterns. Additionally, measurements were performed at room temperature and during heating and cooling of the sample with a Bruker AXS General Area Detector Diffractometer System. The room-temperature measurements were made on a sample sealed in a  $0.5 \text{ mm}$  XRD glass capillary tube with  $0.5 \text{ mm}$  collimator and a sample-to-detector distance of  $30 \text{ cm}$ . Heating and cooling measurements were made on a sample sealed in  $1 \text{ mm}$  glass capillary tube with a sample-to-detector distance of  $15 \text{ cm}$  [13]. The sample was heated and cooled from 323 to 413 K at  $1 \text{ K/min}$  while collecting a diffraction pattern every 120 s.

## 3. Structure determination

### 3.1. Diffraction patterns

The neutron diffraction patterns measured at 100, 200, 300 and 400 K are plotted in Fig. 2. Having many more reflections, the data at the three lower temperatures indicate a more ordered structure. These weak reflections have not been previously reported, do not match any prior results, and do not index to any previously proposed crystal structure. In view of the loss of low intensity peaks we interpret the transformation between

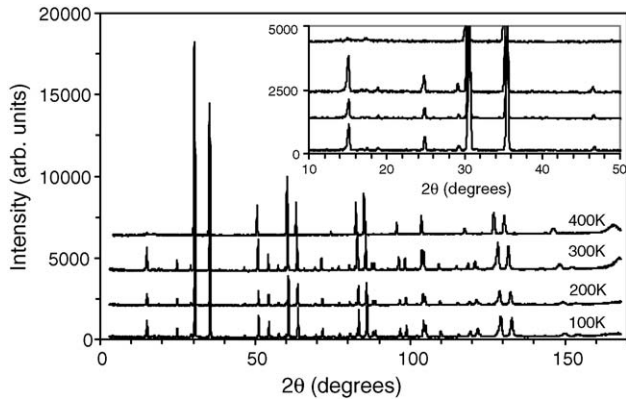


Fig. 2. Neutron diffraction data in the range  $100\text{ K} < T < 400\text{ K}$ . Some differences in intensities are related to differences in the run times. The inset expands the low angle regions.

300 and 400 K as an order–disorder transition. The data at 400 K resemble those reported previously for  $\text{Li}_2\text{NH}$  at room temperature [6–8]. Fig. 3 shows several short measurements made in the direction of decreasing temperature that indicate transformation between 370 and 375 K. Except for small shifts in the positions of the reflections due to thermal expansion, the diffractograms collected at the three lower temperatures are nearly identical.

Fig. 4 shows the X-ray diffractograms measured during heating and cooling. The reflection at  $2\theta = 15^\circ$  is only observed at  $T < 358\text{ K}$ . The broad hump at  $2\theta = 22^\circ$  is due to diffuse scattering from the capillary. During the order–disorder transformation, a transient increase in the intensity of the reflection at  $2\theta = 30^\circ$  was observed; after the transformation was complete, the intensity of the reflection returned to its original value. This phenomenon was not observed during the reverse transformation. A slight sharpening of the reflections at  $2\theta = 30^\circ$  and  $35^\circ$  was observed only during the transformation irrespective of the direction of temperature change. The gradual shifts in the positions of the reflections appeared to be related to thermal expansion rather

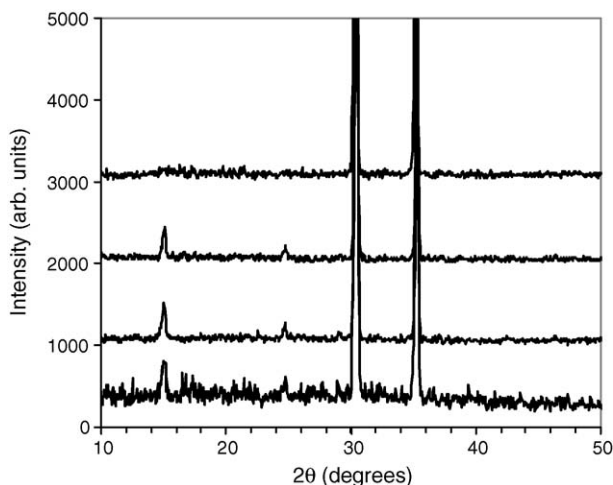


Fig. 3. Neutron diffraction data identifying the transformation temperature; 350 K (bottom), 360 K, 370 K and 375 K (top).

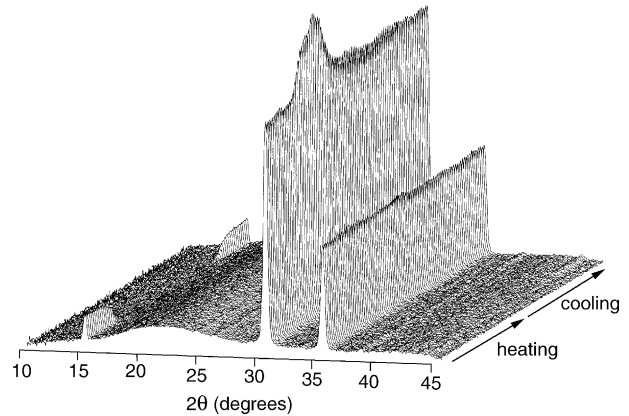


Fig. 4. X-ray diffraction data during heating and cooling of  $\text{Li}_2\text{ND}$  at  $1\text{ K/min}$  from 323 to 413 K, measured in 2 K increments and plotted as the square root of intensity.

than the phase transformation. The neutron (Figs. 2 and 3), X-ray (Fig. 4), and DSC data (Fig. 1) consistently establish an order–disorder transition in  $\text{Li}_2\text{ND}$  in the vicinity of 360 K, in agreement with the work of Forman [9].

### 3.2. Indexing

#### 3.2.1. Low-temperature phase

Indexing results are listed in Table 1 for the neutron and X-ray data. Both sets of data could be indexed as cubic with a lattice constant,  $a$ , of  $10.09\text{--}10.13\text{ \AA}$  in the range 100–300 K. The lattice parameter for the 300 K data,  $a = 10.13\text{ \AA}$ , is approximately twice those reported previously for  $\text{Li}_2\text{NH}$  [6–8]. Thirty-nine reflections from the X-ray data and all thirty-eight reflections in the low-temperature neutron data were indexed. Indexing was performed both graphically and with the program TREOR90 in Crysfire 2002.

The observed reflections could be indexed to a set of all even or all odd indices; therefore, the Bravais lattice type is face-centered. Based on the systematic absences, eight space groups are possible:  $F23$  (1 9 6),  $Fm\bar{3}$  (2 0 2),  $Fd\bar{3}$  (2 0 3),  $F432$  (2 0 9),  $F4_132$  (2 1 0),  $F\bar{4}3m$  (2 1 6),  $Fm\bar{3}m$  (2 2 5), and  $Fd\bar{3}m$  (2 2 7). Having a lattice parameter of  $10\text{ \AA}$  rather than  $5\text{ \AA}$ , the low temperature structure will have  $2^3$  as many formula units as in the previous structure models. This factor, as well as density considerations, requires the crystal structure to contain 32  $\text{Li}_2\text{ND}$  formula units per unit cell.

#### 3.2.2. High-temperature phase

The 16 observed reflections in the neutron diffraction data collected at 400 K were also indexed as cubic, with a lattice constant of  $5.09\text{ \AA}$ , the same as the previously reported room-temperature values for  $\text{Li}_2\text{NH}$  [6–8]; Table 2 details the results. The Miller indices were all even or all odd, once again indicating a face-centered Bravais lattice. The high-temperature phase must therefore contain the same number ( $Z = 4$ ) of formula units as the previously reported structures. Analysis of systematic absences limited the possible space groups to five:  $F23$ ,  $Fm\bar{3}$ ,  $F432$ ,  $F\bar{4}3m$ , and  $Fm\bar{3}m$ .

Table 1  
Indexing results for the low-temperature phase of Li<sub>2</sub>ND

X-ray, room temperature, $a = 10.13088 \text{ \AA}$			Neutron, $T = 100 \text{ K}$ , $a = 10.0850 \text{ \AA}$		
$hkl$	$2\theta$ (°)	$d$ (Å)	$hkl$	$2\theta$ (°)	$d$ (Å)
1 1 1	15.119	5.8551	1 1 1	15.171	5.8227
2 2 0	24.817	3.5847	2 2 0	24.917	3.5656
3 1 1	29.199	3.0560	3 1 1	29.312	3.0407
2 2 2	30.529	2.9258	2 2 2	30.648	2.9113
4 0 0	35.398	2.5337	4 0 0	35.541	2.5212
4 2 2	43.724	2.0686	5 1 1/3 3 3	46.725	1.9409
5 1 1/3 3 3	46.530	1.9502	4 4 0	51.155	1.7828
4 4 0	50.936	1.7913	6 0 0/4 4 2	54.508	1.6808
5 3 1	53.450	1.7128	6 2 0	57.727	1.5946
6 0 0/4 4 2	54.289	1.6883	5 3 3	60.068	1.5379
6 2 0	57.473	1.6022	6 2 2	60.836	1.5204
5 3 3	59.805	1.5451	4 4 4	63.853	1.4556
6 2 2	60.564	1.5276	7 1 1/5 5 1	66.065	1.4122
4 4 4	63.564	1.4625	6 4 2	69.671	1.3477
7 1 1/5 5 1	65.762	1.4189	7 3 1/5 5 3	71.795	1.3129
7 3 1/5 5 3	71.457	1.3191	7 3 3	77.341	1.2321
8 0 0	74.917	1.2665	8 2 2/6 6 0	80.745	1.1885
7 3 3	76.967	1.2378	7 5 1/5 5 5	82.77	1.1645
8 2 2/6 6 0	80.351	1.1940	6 6 2	83.443	1.1568
7 5 1/5 5 5	82.356	1.1699	8 4 0	86.127	1.1275
6 6 2	83.023	1.1622	9 1 1/7 5 3	88.134	1.1070
8 4 0	85.682	1.1328	8 4 2	88.802	1.1004
9 1 1/7 5 3	87.681	1.1121	8 4 4	96.837	1.0293
6 6 4	90.968	1.0803	9 9 3/7 7 1/7 5 5	98.861	1.0136
8 4 4	96.302	1.0341	8 6 0	99.538	1.0085
9 9 3/7 7 1/7 5 5	98.287	1.0184	10 2 0/8 6 2	102.26	0.9889
9 5 1/7 7 3	103.710	0.9794	10 2 2/6 6 6	105.011	0.9704
10 2 2/6 6 6	104.390	0.9749	11 1 1/7 7 5	115.72	0.9093
9 5 3	109.238	0.9448	8 8 0	119.492	0.8914
11 1 1/7 7 5	114.955	0.9135	11 3 1/9 7 1/9 5 5	121.823	0.8811
8 8 0	118.673	0.8955	10 4 4/8 8 2	122.613	0.8778
11 3 1/9 7 1/9 5 5	120.960	0.8852	10 6 0/8 6 6	125.847	0.8648
10 6 0/8 6 6	124.920	0.8687	11 3 3/9 7 3	128.362	0.8554
11 3 3/9 7 3	127.366	0.8594	10 6 2	129.219	0.8523
10 6 2	128.212	0.8563	12 0 0/8 8 4	132.762	0.8404
12 0 0/8 8 4	131.664	0.8443	12 4 0	149.96	0.7973
11 5 1/7 7 7	134.386	0.8356	8 8 6	155.835	0.7875
10 6 4	139.231	0.8217			

### 3.3. Crystal structure models

#### 3.3.1. Low-temperature phase

The compound Li<sub>2</sub>ND is ionic, with [ND]<sup>2-</sup> being larger than Li<sup>+</sup>, so that cubic closest-packing of the anions is expected. Thus, a further reduction of the possible space groups resulted by considering only those with sites whose equivalent positions are in a close-packed configuration and with a multiplicity of 32. This leaves the *F23*, *F4<sub>1</sub>32*, and *F4<sub>3</sub>m* space groups and requires the nitrogen atoms to be located on either the 32e site in the *F4<sub>1</sub>32* and *Fd3m* space groups or on both of two 16e sites in the *F23* and *F4<sub>3</sub>m* space groups. Because of the similarities in the 16e and 32e sites, and because differences in the space groups are not apparent except at sites of higher multiplicity, the *Fd3m* space group, having the highest symmetry, was selected for structure refinement.

To form a structure consistent with the [ND]<sup>2-</sup> anion, D sites were placed at a distance of 1 Å from N on a 32e site at (0.30,

0.30, 0.30). To maintain an anti-fluorite structure, i.e., tetrahedral arrangement of four [ND]<sup>2-</sup> anion nearest neighbors for Li<sup>+</sup>, Li atoms were placed at the 8a and 48f sites. In an ideal anti-fluorite structure, eight Li atoms would be located on the 8b site, but in our model the 8b site is actually tetrahedrally coordinated by deuterium. Therefore, this left eight Li atoms unaccounted for. To determine the most likely position of these atoms, we systematically refined models with these atoms located on the available sites (i.e., 8b, 16c, 16d, 32e, 48f, 48g, and 96h) and set the occupancies accordingly.

#### 3.3.2. High-temperature phase

For the initial structural model of the high-temperature phase the *Fm3m* space group was selected since it has the highest symmetry consistent with the systematic absences, along with the required cubic closest-packed sites with multiplicities of 4. With this space group, site occupancy is maximized by either placing the N atoms or D atoms on the 4a sites and the Li atoms

Table 2  
Indexing results for the high-temperature phase of Li<sub>2</sub>ND

Neutron, $T=400$ K, $a=5.0904$ Å		
$hkl$	$2\theta$ (°)	$d$ (Å)
1 1 1	30.366	2.9389
2 0 0	35.209	2.5452
2 2 0	50.653	1.7997
3 1 1	60.217	1.5348
2 2 2	63.196	1.4695
4 0 0	74.463	1.2726
3 3 1	82.499	1.1678
4 2 0	85.137	1.1382
4 2 2	95.643	1.0391
5 1 1	103.631	0.9796
3 3 3	103.631	0.9796
4 4 0	117.682	0.8999
5 3 1	127.007	0.8604
4 4 2	130.368	0.8484
6 0 0	130.368	0.8484
6 2 0	146.186	0.8049
5 3 3	165.524	0.7763

on the 8c sites. To determine the positions of the remaining atoms, a series of models was tested, where in a given model the remaining atoms were placed on one or two of the remaining available sites (4b, 24d, 24e, 48g, 48h, 48i, 96j, 96k, and 192l). The fractional occupancies were adjusted accordingly to  $4/m_s$  (one-site model) or  $4/(m_{s1} + m_{s2})$  (two-site model) where  $m_s$  is the site multiplicity.

### 3.4. Refinements

#### 3.4.1. Neutron diffraction

Refinement of the neutron diffraction data was performed with the general structure analysis system (GSAS) [14] suite of programs and the EXPGUI [15] graphical user interface to GSAS. In the initial stages of the refinement, satisfactory fits to the scale factor, background, lattice parameters, diffractometer zero, and peak profiles for both phases were obtained from LeBail fits [16] to the full intensities of the reflections. Next, Rietveld refinement of a structure model containing Li on the 8a and 48f sites, N and D was performed on total intensity versus  $2\theta$  with scale factor and background (a Chebyshev polynomial), lattice parameters, diffractometer zero, peak profiles (Gaussian modified for peak asymmetry), fractional atomic coordinates ( $x, y, z$ ), and atomic displacement parameters ( $U_{iso}$ ). Given the total masses and number densities of Li, N and D in the sample, the neutron absorption cross sections for the elements were sufficiently low that an absorption correction was not necessary. Parameters were refined to convergence, i.e., until the shifts in the parameters were 1% or less of the estimated standard deviation.

To determine the most probable low temperature crystal structure model, we systematically refined models with eight unaccounted Li atoms located on the available sites (i.e., 8b, 16c, 16d, 32e, 48f, 48g, and 96h) and set the occupancies accordingly. The model with the lowest weighted profile factor  $R_{wp}$  has the eight Li atoms placed on the 32e (0.04, 0.04, 0.04) site. This was

also the only model where the Li occupancy  $f$  refined to  $>0.0$ . The structural parameters at 100, 200, and 300 K for our refinements with the lowest  $R_{wp}$  are listed in Table 3, the refinement results at 100 K are shown in Fig. 5, and the structure model is shown in Fig. 8(a). The nitrogen atoms are slightly displaced from a close-packed configuration ( $x = 0.25$ ); this displacement results in the ND<sup>-2</sup> dyad being more centered on these sites. The Li 32e to Li 32e interatomic distance ( $<1.5$  Å) is small but these sites have a low occupancy, making it unlikely that adjacent sites are simultaneously occupied. At 100 K the Li occupancy on the 32e site refined to 0.32. This is larger than would be expected from the stoichiometry but is in good agreement with the chemical analysis. Charge balance of the excess Li suggests the possible existence of nitrogen and hydrogen atoms in the form of nitride (N<sup>3-</sup>) and hydride (H<sup>1-</sup>) anions as is found in the Li<sub>4</sub>NH structure [17]. The atomic displacement parameters are consistent with those for LiNH<sub>2</sub>, with H being the largest and N the smallest.

The refinements at the three temperatures show good relative agreement. As expected, the lattice expands linearly with temperature. At 200 K the atomic coordinates, Li site occupancy, and interatomic distances are identical to those at 100 K, and the atomic displacement parameters increase only modestly. At 300 K the refined parameters show a considerable change from those at both 100 and 200 K. The atomic coordinates for the nitrogen and deuterium atoms show that both have moved towards the close-packed configuration resulting in an unexpected shortening in the N–D distance. The Li atoms on the 32e sites have moved towards the 16d sites, which are octahedrally coordinated by nitrogen, and the refined occupancy is closer to the ideal stoichiometry. Lastly, the atomic displacement parameters have all increased substantially, with the largest increase for the Li on the 32e sites which at 300 K surpasses that for deuterium. These changes all suggest a loss in the low temperature structural stability above 300 K.

Refinement results for the 400 K data are reported in Table 4. For brevity only the models with an  $R_{wp}$  of less than 0.09 are listed. Even though physically unlikely, Model 6 with the D atoms located on the 4a sites and the N on the 32e sites gives

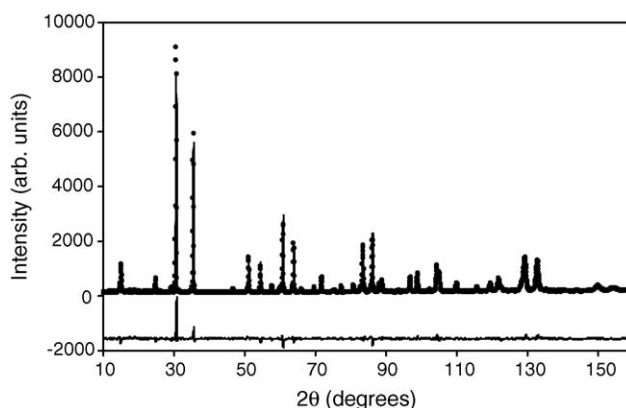


Fig. 5. Refinement results for neutron diffraction data at 100 K (observed (●), calculated (—) and difference (below) patterns).

Table 3

Comparison of structural parameters for the low-temperature Li<sub>2</sub>ND phase refined with space group *Fd* $\bar{3}m$  (origin 2)

Method	Neutron			X-ray	
<i>T</i> (K)	100	200	300	Room temperature	Room temperature
<i>a</i> (Å)	10.08728(18)	10.1035(9)	10.1268(10)	10.12971(7)	10.12988(6)
Scale	2479(17)	1764(14)	3662(29)		
<i>R</i> <sub>wp</sub>	9.03%	9.80%	8.93%	8.81%	7.69%
<i>R</i> <sub>p</sub>	7.62%	8.15%	7.42%	6.35%	5.65%
$\chi^2_r$	2.057	1.773	3.131	2.81	2.45
N, 32e, <i>f</i> =1					
Scattering factor	N	N	N	N	O <sup>1-</sup>
<i>x</i>	0.24178(5)	0.24176(6)	0.24222(6)	0.2461(1)	0.2432(1)
<i>U</i> <sub>iso</sub> × 100	−0.03(2)	0.14(3)	0.41(3)	1.20(2)	0.94(3)
D, 32e, <i>f</i> =1					
<i>x</i>	0.29762(14)	0.29742(16)	0.29659(18)	0.2828(11)	0.2846(11)
<i>U</i> <sub>iso</sub> × 100	3.13(6)	3.42(7)	4.66(8)	−0.2(5)	1.4(7)
Li1, 48f, <i>f</i> =1					
<i>x</i>	0.3734(5)	0.3740(6)	0.3702(7)	0.3640(6)	0.3725(3)
<i>U</i> <sub>iso</sub> × 100	2.12(9)	2.36(10)	3.18(12)	5.30(7)	2.52(5)
Li2, 8a, <i>f</i> =1					
<i>U</i> <sub>iso</sub> × 100	0.6(3)	0.6(3)	1.1(3)	−0.84(6)	0.67(15)
Li3, 32e					
<i>x</i>	0.0376(12)	0.0387(16)	0.030(2)	0.010(7)	0.0316(8)
<i>U</i> <sub>iso</sub> × 100	1.4(6)	1.0(5)	6.5(18)	14.3 (16)	3.1(6)
<i>f</i>	0.32(3)	0.30(3)	0.26(3)	0.299(15)	0.252(11)
Interatomic distances					
N–D	0.977	0.975	0.956	0.644	0.726
N–Li					
48f	2.244	2.244	2.267	2.280	2.249
48f	2.131	2.138	2.121	2.106	2.141
8a	2.041	2.043	2.056	2.125	2.074
32e	2.098	2.095	2.157	2.605	2.173
D–Li					
48f	2.075	2.072	2.109	2.161	2.091
	2.58	2.583	2.569	2.406	2.454
Li–Li					
48f–48f	2.522	2.526	2.533	2.537	2.533
48f–32e	2.048	2.056	2.038	2.070	2.056
48f–32e	2.483	2.497	2.419	2.205	2.425
48f–8a	2.507	2.517	2.484	2.421	2.507
32e–8a	1.515	1.504	1.632	2.012	1.639
32e–8a	2.853	2.871	2.753	2.374	2.748
32e–32e	1.338	1.37	1.12	0.360	1.110
32e–32e	2.474	2.46	2.67	3.290	2.680
Composition (%)					
N	46.1	46.3	46.8	46.3	46.8
D	6.6	6.6	6.7	6.6	6.7
Li	47.3	47.1	46.6	47	46.5

the lowest *R*<sub>wp</sub>. Subsequent DFT modeling confirmed that this structure is doubtful and, therefore, it was not considered as the most likely high temperature phase. Of the remaining Models, 4 and 5 gave substantially lower *R*<sub>wp</sub> than Models 1–3. These two models have comparable interatomic distances and show little difference except the site multiplicity of the D atom. Intuitively, one might prefer the model with the lower multiplicity (higher D occupancy), but thermodynamically the model with the larger multiplicity (lower occupancy) would have the larger config-

urational entropy, making it the more stable phase at elevated temperatures. Lastly, the Li–D interatomic distance in Model 5 is larger and agrees better with the low temperature phase. Therefore, given that Model 5 refines to a slightly lower *R*<sub>wp</sub>, is expected to be more thermodynamically stable at high temperatures, and has the larger Li–D interatomic distance, we feel Model 5 is the more likely structure at 400 K. The refinement results at 400 K for Model 5 are shown in Fig. 6, and the corresponding structure is shown in Fig. 8(b).

Table 4  
Comparison of neutron diffraction refinement results for  $\text{Li}_2\text{ND}$  at 400 K with space group  $Fm\bar{3}m$  and D atoms placed at various sites

Model	1	2	3	4	5	6
$a$ (Å)	5.09187	5.09188	5.09172	5.09189	5.09187	5.09188
Scale	27652	25421	25641	27344	28249	30520
$R_{\text{wp}}$	8.01%	8.12%	8.04%	7.29%	7.11%	7.02%
$R_{\text{p}}$	6.61%	6.65%	6.63%	6.11%	6.00%	5.94%
$\chi^2_r$	2.172	2.219	2.184	1.79	1.71	1.669
N						
Site	4a	4a	4a	4a	4a	32f
$x$	0	0	0	0	0	0.0791
$U_{\text{iso}} \times 100$	1.714	1.351	1.354	1.558	1.645	8.658
$f$	1	1	1	1	1	0.125
Li, 8c, $f=1$						
$U_{\text{iso}} \times 100$	5.138	5.093	5.085	4.966	5.141	5.496
D						
Site	32f	48h	96j	96k	192l	4a
$x$	0.0990	0	0.1054	0.0702	0.1426	0
$y$	0.0990	0.1155	0.1252	0.0702	0.0928	0
$z$	0.0990	0.1155	0	0.1420	0.0509	0
$U_{\text{iso}} \times 100$	6.959	4.447	4.402	2.213	1.503	0.278
$f$	0.125	0.0833	0.0417	0.0417	0.0208	1
Interatomic distances in Å						
$r(\text{N-D})$	0.77	0.828	0.831	0.882	0.904	0.697
$r(\text{Li-D})$	1.435	1.602	1.604	1.407	1.403	2.205
$r(\text{Li-N})$	2.205	2.205	2.205	2.205	2.205	1.508

### 3.4.2. X-ray diffraction

Refinement of the room-temperature X-ray data was performed by the Rietveld method with the program RIQAS. Since an X-ray atomic scattering factor is not readily available for  $\text{N}^{2-}$ , Rietveld refinement of the X-ray data is inherently less accurate. Refinements using a neutral nitrogen scattering factor resulted in a slight disparity with the atomic positions obtained from the neutron measurements. Use of a scattering factor for an atom or ion ( $\text{O}^{1-}$ , F) isoelectronic with  $\text{N}^{2-}$  improves the agreement between the X-ray and neutron atomic parameters as well as the quality of the fit. Alternatively, approximate correction for the N scattering factor can be made by refining the N occupancy. This approach also improves the agreement between the atomic parameters determined from the X-ray and neutron

data and the quality of the fit, but the N occupancy factor refines to  $>1$ . The refinement results for the room-temperature X-ray data are shown in Fig. 7 with atomic scattering factor for neutral N. The refined parameters are summarized in Table 3 for neutral N and  $\text{O}^{1-}$  atomic scattering factors both with the occupancy factor set to 1. There is good agreement between neutron and X-ray data for the lattice parameter, N atomic position, Li 48f atomic position, and some atomic displacement parameters, but poorer agreement for many of the other values. These discrepancies may only be an artifact arising from the use of a neutral N X-ray scattering factor. The X-ray refinements also indicate a very short N–D distance. This might reflect a difference in the nuclear position and the charge density center and/or inferior accuracy of the X-ray refinements.

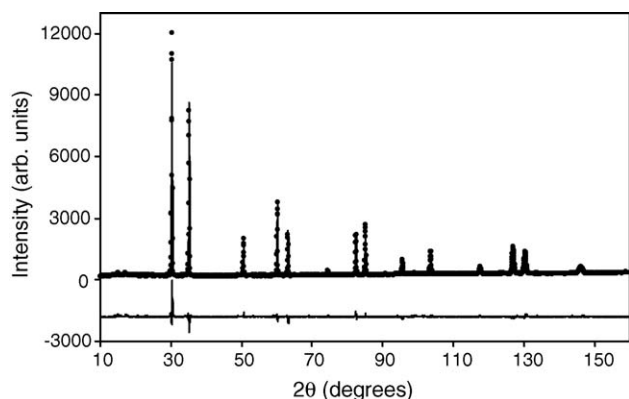


Fig. 6. Refinement results for  $\text{Li}_2\text{ND}$  neutron diffraction data at 400 K (observed (●), calculated (—) and difference (below) patterns).

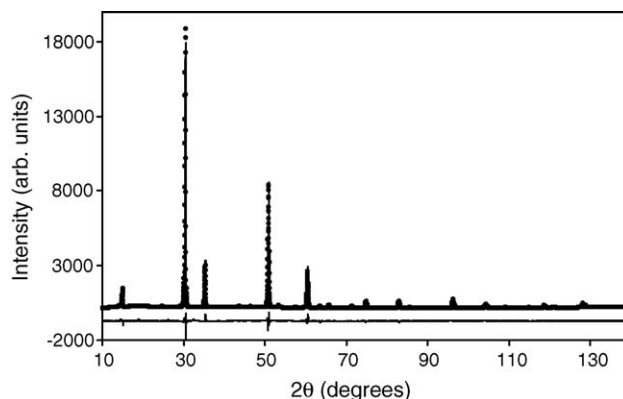


Fig. 7. Refinement results for the  $\text{Li}_2\text{ND}$  room temperature X-ray data (observed (●), calculated (—) and difference (below) patterns).

Table 5

Space group, volume  $V$ , minimum nearest-neighbor distances, and unrelaxed and relaxed total energies from DFT calculations for fully occupied models of the low temperature  $\text{Li}_2\text{NH}$  crystal structure

Space group	$V$ ( $\text{\AA}^3/\text{Li}_2\text{NH}$ )	Minimum nearest-neighbor distances ( $\text{\AA}$ )					$E$ (eV/ $\text{Li}_2\text{NH}$ )	
		Li–H	Li–N	H–N	Li–Li	H–H	Unrelaxed	Relaxed
$Fd\bar{3}m$ (227) [Li at 8a, 8b]	37.59	1.567	2.024	1.014	2.376	2.559	–16.902	–16.943
$Fd\bar{3}m$ (227) [Li at 16c]	30.63	1.969	2.156	1.044	2.197	2.018	–17.176	–17.310
$Fd\bar{3}m$ (227) [Li at 16d]	32.37	2.097	2.009	1.027	2.466	1.784	–16.253	–17.383
$Imm2$ (44)	31.77	1.965	1.961	1.035	2.217	1.996	–17.597	–17.609
$Ima2$ (46)	31.76	1.964	1.960	1.035	2.218	1.998	–17.136	–17.609
$R\bar{3}m$ (166)	42.83	2.152	1.850	1.035	2.028	2.664	–16.692	–17.470
$Imm2$ (44) [equivalent to Noritake]	32.19	1.788	2.134	1.034	2.312	3.285	–15.162	–17.391
$R\bar{3}m$ (160) [equivalent to Ohoyama]	33.78	1.760	2.069	1.029	2.386	3.595	–15.503	–17.293

The volumes and distances are from the relaxed calculations.

#### 4. Equivalent fully occupied structures and DFT modeling of $\text{Li}_2\text{NH}$

In the interest of tractability as well as to obviate uncertainties associated with treating partial occupancy of high multiplicity sites in large unit cells, we first identified, by means of two different approaches, fully occupied low-temperature structures whose total energy could be calculated in a straightforward manner. The first approach eliminated partial occupancy of the Li

32e site in the  $Fd\bar{3}m$  structure refined from the 100 K neutron data (Table 3) via three models having, in addition to those at the 48f positions, Li atoms completely populating the (1) 8a and 8b, (2) 16c, or (3) 16d sites. In the second approach 28 lower symmetry configurations were generated by placing two Li atoms in all 28 combinations of two of the eight 32e sites in the primitive unit cell. Interestingly, analysis of these yielded three distinct, fully occupied structures having orthorhombic ( $Ima2$ ,  $Imm2$ ) and rhombohedral ( $R\bar{3}m$ ) symmetries. The existence of

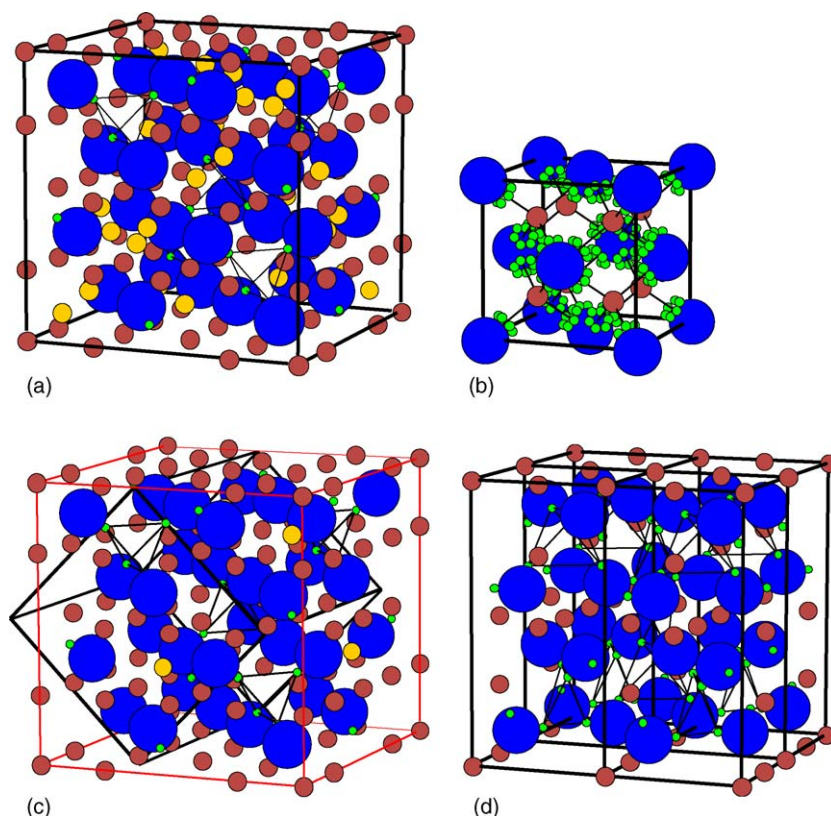


Fig. 8. Structure models for (a) cubic low-temperature  $\text{Li}_2\text{ND}$  phase; (b) high-temperature  $\text{Li}_2\text{ND}$  phase; (c) fully occupied orthorhombic  $Ima2$  equivalent low-temperature  $\text{Li}_2\text{ND}$  phase; (d) lithium amide  $\text{LiND}_2$  at room temperature. The internal tetrahedra show deuterium coordination to vacant tetrahedral sites. The chords between N and Li atoms in (b) highlight the hexagonal arrangement of the partially occupied D sites. To facilitate comparison with the low-temperature amide  $\text{Li}_2\text{ND}$  structure (a), the original partially occupied cubic lattice (red lines) and the fully occupied orthorhombic lattice (thick black lines) are shown (c) and four cells of the  $\text{LiND}_2$  structure are displayed in (d). Blue = N, Green = D, Brown = tetrahedrally coordinated Li; and Yellow = non-tetrahedrally coordinated Li.

fully occupied equivalents is consistent with the naïve expectation that the lowest temperature structure of  $\text{Li}_2\text{NH}$  should be an array of  $\text{Li}_2\text{NH}$  units, as is the case for lithium amide,  $\text{LiNH}_2$ .

Optimized electronic total energies and structural parameters for the six fully occupied low temperature  $\text{Li}_2\text{NH}$  structures were obtained with the Vienna ab initio simulation package (VASP) using projector augmented-wave potentials with the generalized gradient approximation for the exchange-correlation energy functional. VASP implements density functional theory (DFT) [18] utilizing a plane wave basis set [19,20]. The lattice parameters and nuclear coordinates were allowed to fully relax during the course of the calculations. The cell volume  $V$ , minimum nearest-neighbor distances, and total energies  $E$  from the relaxation calculations are summarized in Table 5; the unrelaxed energies, those obtained with the input crystal structures, are also included. The results are consistent with the neutron diffraction data. In all cases, the N–H distance always relaxed to  $>1 \text{ \AA}$ , close to the N–D distance obtained from the neutron diffraction data. The slight difference might be due to the fact that the VASP values are for 0 K and were calculated from structures with ideal  $\text{Li}_2\text{NH}$  stoichiometry whereas the neutron results were obtained on  $\text{Li}_2\text{ND}$  at higher temperatures and from a sample rich in Li. The models with the lowest total electronic energy were the three derived from ordering the Li atoms on the 32e site, while those derived from the repositioning of these Li atoms on other sites had higher energies. Additionally, the two orthorhombic models have the same, and lowest, total energy and yield normalized cell volumes very close to the value ( $32.08 \text{ \AA}^3/\text{Li}_2\text{NH}$ ) from the 100 K diffraction data. The *Ima2* structure has fewer atomic sites (12) than the *Imm2* structure (17); Table 6 lists the input and VASP relaxed structural parameters for the former, and Fig. 8(c) is a diagram of the structure.

We also analyzed the fcc models proposed by Ohoyama et al. [7] and Noritake et al. [8]. In each case we constructed the conventional cubic cell with the hydrogen sites fully occupied, transformed to the primitive cell, and built coordinate sets having the  $\text{Li}_2\text{NH}$  stoichiometry by populating only one H at a time in the primitive cell. This procedure yields four possibilities for the Model II  $F\bar{4}3m$  structure (H at 16e) preferred by Ohoyama et al. [7] and 12 possibilities for the  $Fm\bar{3}m$  structure (hydrogen at 48h sites) of Noritake et al. [8]. We find that all four representations of Model II of Ohoyama et al. [7] are equivalent to a single fully occupied rhombohedral ( $R\bar{3}m$ ) lattice, and the 12 representations of the Noritake et al. [8] structure are equivalent to one orthorhombic (*Imm2*) lattice. That is, the powder diffraction patterns of the partially occupied cubic structures of Ohoyama et al. [7] and Noritake et al. [8] are precisely the same as the patterns for fully occupied rhombohedral and orthorhombic lattices, respectively. The two structures were fully relaxed with VASP. Tables 7 and 8 list the input and relaxed structural parameters, and the corresponding total energies are included in Table 5. It is clear from Table 5 that the structures of Ohoyama et al. [7] and Noritake et al. [8] are characterized by unrelaxed energies higher than any others, and they also lead to relaxed energies higher than either of the two orthorhombic structures

Table 6

Input and relaxed structural parameters for the fully occupied orthorhombic lattice (*Ima2*; space group No. 46) equivalent to the partially occupied 100 K structure of Table 3

	Input	Calculated (VASP relaxed)
$a$ (Å)	7.133	7.118
$b$ (Å)	10.087	10.072
$c$ (Å)	7.133	7.088
Li1 (4b)		
$y$	0.3734	0.3826
$z$	0.3750	0.3703
Li2 (4b)		
$y$	0.8766	0.8765
$z$	0.3750	0.3703
Li3 (4b)		
$y$	0.1250	0.1058
$z$	0.3750	0.3705
Li4 (4b)		
$y$	0.2876	0.2498
$z$	0.0499	0.1206
Li5 (8c)		
$x$	0.4984	0.5074
$y$	0.1250	0.1155
$z$	0.1266	0.1372
Li6 (8c)		
$x$	0.4984	0.5073
$y$	0.3750	0.3844
$z$	0.1234	0.1034
N1 (4b)		
$y$	0.0082	0.0087
$z$	0.6086	0.6101
N2 (4b)		
$y$	0.0082	0.0089
$z$	0.1414	0.1305
N3 (8c)		
$x$	0.4836	0.4691
$y$	0.2418	0.2405
$z$	0.3750	0.3700
H1 (4b)		
$y$	0.5476	0.5505
$z$	0.2203	0.2295
H2 (4b)		
$y$	0.5476	0.5506
$z$	0.5297	0.5114
H3 (8c)		
$x$	0.5953	0.5819
$y$	0.2024	0.1945
$z$	0.8750	0.8700

The conventional orthorhombic cell contains 16  $\text{Li}_2\text{NH}$  formula units.

corresponding to our 100 K neutron data. Also, the  $\sim 0.8 \text{ \AA}$  H–N nearest neighbor distance characterizing both initial structures [7,8] expands to  $1.03 \text{ \AA}$  in the relaxed versions.

Via similar analyses we have found that each of the high temperature  $\text{Li}_2\text{NH}$  structures in Table 4 is equivalent, again in the sense of generating identical powder diffraction patterns, to lower symmetry, fully occupied structures. Table 9 presents results analogous to those of Table 5. All the relaxed ener-

Table 7

Input and relaxed structural parameters for the fully occupied rhombohedral lattice ( $R3m$ ; space group No. 160) equivalent to the partially occupied fcc Model II structure of Ohoyama et al. [7] ( $F\bar{4}3m$ ; space group No. 216;  $a = 5.0769$  Å; Li at 4c and 4d; N at 4a; 4 H at 16e with  $x = 0.093$ )

	Input (equivalent to Ohoyama Model II)	Calculated (VASP relaxed)
$a$ (Å)	3.5899	3.5951
$c$ (Å)	8.7935	9.0541
Li1 (3a) $z$	0.5745	0.6584
Li2 (3a) $z$	0.0745	0.1218
N (3a) $z$	0.3245	0.3503
H (3a) $z$	0.4175	0.464

The hexagonal representation ( $\alpha = \beta = 90^\circ$ ,  $\gamma = 120^\circ$ ) is used; the unit hexagonal cell contains three  $\text{Li}_2\text{NH}$  formula units.

Table 8

Input and relaxed structural parameters for the fully occupied orthorhombic lattice ( $Imm2$ ; space group No. 44) equivalent to the partially occupied fcc structure of Noritake et al. [8] ( $Fm\bar{3}m$ ; space group No. 225;  $a = 5.0742$  Å; Li at 8c; N at 4a; 4 H at 48 h with  $y = 0.11$ )

	Input (equivalent to Noritake)	Calculated (VASP relaxed)
$a$ (Å)	3.588	3.5648
$b$ (Å)	5.0742	5.4978
$c$ (Å)	3.588	3.2846
Li (4d)		
$y$	0.25	0.2103
$z$	0.09	0.9302
N (2b) $z$	0.59	0.4922
H (2b) $z$	0.37	0.1775

The conventional orthorhombic cell contains two  $\text{Li}_2\text{NH}$  formula units.

gies in Table 9 are higher than the lowest relaxed energies ( $-17.609$  eV/ $\text{Li}_2\text{NH}$ ) of the low temperature models listed in Table 5, consistent with the fact that the 400 K structure must be inherently less stable. Models 1 and 6 can be represented by  $R3m$  structures whose relaxed total energies are identical to each other and to that of the equivalent low temperature model of Ohoyama et al. [7] in Table 5; the initial structures are very distinct, however, as are their unrelaxed energies. The same is true for the  $Imm2$  equivalent of Model 2 and the Noritake et al. [8] model in Table 5. Models 3 and 4 can each be represented by a monoclinic ( $Cm$ ) structure, while Model 5 is equivalent to a triclinic structure which yields the same relaxed energy. Consid-

Table 9

Space group, volume  $V$ , minimum nearest-neighbor distances, and unrelaxed and relaxed total energies from DFT calculations for fully occupied equivalents of the high temperature (HT)  $\text{Li}_2\text{NH}$  crystal structure models of Table 4

HT Model equivalent space group	$V$ (Å <sup>3</sup> / $\text{Li}_2\text{NH}$ )	Minimum nearest-neighbor distances (Å)					$E$ (eV/ $\text{Li}_2\text{NH}$ )	
		Li–H	Li–N	H–N	Li–Li	H–H	Unrelaxed	Relaxed
Model 1 $R3m$ (160)	33.79	1.759	2.072	1.029	2.386	3.595	-16.127	-17.293
Model 2 $Imm2$ (44)	32.21	1.788	2.135	1.034	2.314	3.286	-15.896	-17.391
Model 3 $Cm$ (8)	31.59	1.843	2.143	1.039	2.354	3.499	-15.928	-17.494
Model 4 $Cm$ (8)	31.56	1.841	2.143	1.039	2.351	3.498	-16.389	-17.494
Model 5 $P1$ (1)	31.58	1.841	2.143	1.040	2.354	3.498	-16.550	-17.494
Model 6 $R3m$ (160)	33.76	1.758	2.071	1.029	2.386	3.594	-11.510	-17.293

The volumes and distances are from the relaxed calculations.

ering the goodness-of-fit parameters as well as the interatomic distances in Table 4, we view Model 5 as the best for the high temperature  $\text{Li}_2\text{NH}$  structure. If we make the physical assumption that the structure is likely to be disordered at 400 K, then the partially occupied representation of it in Table 4 is preferable to its fully occupied triclinic equivalent.

## 5. Discussion

Although our low temperature  $\text{Li}_2\text{ND}$  structure model is quite distinct from previously proposed models, it compares favorably with that of lithium amide ( $\text{LiND}_2$ ) [21]. For a direct comparison, the amide  $\text{LiND}_2$  structure is shown with four unit cells in Fig. 8(d). As can be seen in Fig. 8(a) for the low temperature  $\text{Li}_2\text{ND}$  phase and in Fig. 8(d) for  $\text{LiND}_2$ , both have the same basic architecture. That is, they have a slightly distorted cubic closest-packing of the N atoms with only the requisite number of D atoms as nearest neighbors, and all the D atoms are in fully occupied sites with a  $\sim 1$  Å N–D interatomic distance. Additionally, the D atoms in both structures only coordinate with unoccupied tetrahedral sites, and the remaining tetrahedral sites are occupied by Li atoms. Because of geometrical restrictions, the tetrahedral sites only accommodate up to four D atoms or one Li atom. Thus, the number of tetrahedral sites in  $\text{Li}_2\text{ND}$  is insufficient to accommodate all of the Li and D atoms and the excess Li atoms, shown in red, are displaced to partially occupied 32e sites. Lastly, the interatomic distances in Table 3 compare quite favorably with those for  $\text{LiND}_2$  (Li–D: 0.99–1.00 Å, N–Li: 2.06–2.21 Å, D–Li: 2.30–2.95 Å, Li–Li: 2.52 Å, and H–H: 2.34–2.74 Å) [21].

The low-temperature structure model for  $\text{Li}_2\text{ND}$  derived from our diffraction data is quite different than the models recently proposed by Ohoyama et al. [7] and Noritake et al. [8]. The discrepancy with Ohoyama et al. [7] appears to be a consequence of a different indexing choice. All of the peaks observed by Ohoyama et al. [7], including the unassigned peak at  $2\theta = 80^\circ$ , can be indexed by simply doubling the lattice parameter. By doing so the  $2\theta = 80^\circ$  peak indexes to the (5 5 1)/(7 1 1) reflection and is consistent with our proposed structure. The larger unit cell probably was not considered because their data was collected over a limited angular range which did not permit the observation of the (1 1 1) reflection from the larger unit cell, and the data was collected on a non-deuterated sample resulting in a high

background intensity and poor detection of weaker diffraction peaks.

In the case of the work by Noritake et al. [8], no unidentified diffraction peaks were reported so we suspect the discrepancy lies elsewhere. One possibility is a difference in the sample composition. Both the chemical analysis and refinement results indicate that our sample is Li rich. The large  $\text{Li}_2\text{O}$  contamination in Noritake's sample precluded any meaningful chemical analysis, but their structure refinement did give a site occupancy for Li of 0.95, suggesting that their material is Li poor. The lower temperature used to prepare their sample may have been insufficient to fully remove the excess ammonia evolved in the conversion of  $\text{LiNH}_2$  to  $\text{Li}_2\text{NH}$  (Eq. (3)), leaving a small concentration of  $\text{NH}_2^{1-}$  anions in their material. Because of the additional geometric constraints associated with the  $\text{NH}_2^{1-}$  triad, it is not unreasonable to assume that a small substitution of  $\text{NH}_2^{1-}$  would produce a disordered  $\text{Li}_2\text{NH}$  structure.

Near 358 K  $\text{Li}_2\text{ND}$  goes through an order–disorder transformation. During this transformation the Li atoms move from the 32e sites to the unoccupied tetrahedral sites, displacing the four tetrahedrally coordinated D atoms. Surprisingly, the refinement results show that the D atoms do not relocate to sites with a large Li–D interatomic distance (e.g., 24e sites) but, as shown in Fig. 8(b), move only slightly (0.35 Å, with a  $\sim 21^\circ$  rotation from  $\langle 1\ 1\ 1 \rangle$ ) to 192i sites. Even though our proposed high temperature structure has the shortest Li–D interatomic distance (30% smaller than the low temperature phase), the VASP calculations show that the derivative structure of this model has both the lowest unrelaxed and relaxed energies of all the high temperature models considered (Table 9). In fact, these energies are even lower than the corresponding values for the structure models proposed by Ohoyama et al. [7] and Noritake et al. [8] (Table 5).

## 6. Conclusions

Neutron and X-ray diffraction results show the low temperature crystal structure of lithium imide has a space group symmetry of  $Fd\bar{3}m$  with a lattice constant of 10.09–10.13 Å in the range of 100–300 K, twice the previously reported value. Structure refinements show that the  $\text{NH}_2^{2-}$  anions are arranged in a close-packed configuration. Both the N and H atoms are located on fully occupied 32e sites with the H atoms tetrahedrally coordinated to vacant 8b sites and the N atoms tetrahedrally coordinated to Li atoms on the 8a and 48f sites. At 100 K, the N–D interatomic distance is 0.977 Å. The remaining Li atoms are located on partially occupied 32e sites. We have also found, however, that the low temperature phase can be described as a fully

occupied orthorhombic structure to the same degree of accuracy. Single crystal measurements will be necessary to definitively establish the space group.

In the vicinity of 358 K lithium imide exhibits an order–disorder transformation. The high temperature structure has a space group symmetry of  $Fm\bar{3}m$  (anti-fluorite type) with a lattice constant of 5.0919 Å at 400 K. The D atoms randomly occupy 192i sites. DFT results are consistent with the structure refinements.

## Acknowledgements

The authors are grateful to Frederick Pinkerton for DSC measurements, Noel Potter for elemental analyses, Stephen Swarin for helpful discussions, and James Spearot and Mark Verbrugge for their support.

## References

- [1] O. Ruff, F. Georges, Ber. Dtsch. Chem. Ges. 44 (1911) 504.
- [2] F.W. Dafert, R. Miklauz, Mh. Chem. 33 (1912) 65.
- [3] P. Chen, Z. Xiong, J. Luo, J. Lin, K.L. Tan, Nature 420 (2002) 302.
- [4] Y.H. Hu, E. Ruckenstein, J. Phys. Chem. A 107 (2003) 9739.
- [5] T. Ichikawa, N. Hanada, S. Isobe, H. Leng, H. Fujii, J. Phys. Chem. B 108 (2004) 7887.
- [6] R. Juza, K. Opp, Z. Anorg. Allgem. Chemie 266 (1951) 325.
- [7] K. Ohoyama, Y. Nakamori, S. Orimo, K. Yamada, J. Phys. Soc. Jpn. 74 (2005) 483.
- [8] T. Noritake, H. Nozaki, M. Aoki, S. Towata, G. Kitahara, Y. Nakamori, S. Orimo, J. Alloys Compd. 393 (2005) 264.
- [9] R. Forman, J. Chem. Phys. 55 (1971) 1987.
- [10] V.F. Sears, Neutron News 3 (1992) 26.
- [11] Certain commercial materials are identified in this paper to foster understanding. Such identification does not imply recommendation or endorsement by the National Institute of Standards and Technology, nor does it imply that the materials identified are necessarily the best available for the purpose.
- [12] The instrument is described in the NCRN WWW site (<http://www.ncnr.nist.gov/>).
- [13] M.P. Balogh, G.G. Tibbetts, F.E. Pinkerton, G.P. Meisner, C.H. Olk, J. Alloys Compd. 350 (2003) 136.
- [14] A.C. Larson, R.B. Von Dreele, General Structure Analysis System, LAUR 86-748, Los Alamos National Laboratory, 1986.
- [15] B.H. Toby, J. Appl. Cryst. 34 (2001) 210.
- [16] A. LeBail, H. Duroy, J.L. Fourquet, Mater. Res. Bull. 23 (1988) 447.
- [17] R. Niewa, D.A. Zhrebtsov, Z. Kristallogr., New Cryst. Struct. 217 (2002) 317.
- [18] W. Kohn, L. Sham, Phys. Rev. 140 (1965) A1133.
- [19] G. Kresse, J. Hafner, Phys. Rev. B 49 (1994) 14251.
- [20] G. Kresse, J. Furthmüller, Comput. Mater. Sci. 6 (1996) 15.
- [21] M. Nagib, H. Jacobs, Atomkernenergie 21 (1973) 275.